Supporting Information

Electron Paramagnetic Resonance Spectroscopic Identification of the Fe–S Clusters in the SPASM Domain-Containing Radical SAM Enzyme PqqE

Lizhi Tao[1#], Wen Zhu[2#], Judith P. Klinman[2]* and R. David Britt[1]*

[1]Department of Chemistry, University of California, Davis, California 95616, United States

[2]Department of Chemistry, Department of Molecular and Cell Biology, and California Institute for Quantitative Biosciences, University of California, Berkeley, California 94720, United States

*Corresponding Authors: *klinman@berkeley.edu* and *rdbritt@ucdavis.edu*

Table of Contents

Table S1 Primers and DNA templates used in the mutagenesis in this study.

Primer	Sequence	DNA template
C28A forward	5'- GTT AAC GCA CCG TGC TCC ATT GCG TTG C -3'	wild-type
C28A reverse	5'- GCA ACG CAA TGG AGC ACG GTG CGT TAA C -3'	
C28A/C32A/C35A forward	5'- CAC CGT GCT CCA TTG CGT GCC CCT TAT GCT AGT AAT C -3'	C28A
C28A/C32A/C35A reverse	5'- GAT TAC TAG CAT AAG GGG CAC GCA ATG GAG CAC GGT G -3'	
C28A/C32A/C35A/D319H forward	5'- GAT CGT CGT GAG AAA CAT TGG GGG GGA TGT C -3'	C28A/C32A/C35A
C28A/C32A/C35A/D319H reverse	5'- GAC ATC CCC CCC AAT GTT TCT CAC GAC GAT C -3'	
C28A/C32A/C35A/D319C forward	5'- GAT CGT CGT GAG AAA TGT TGG GGG GGA TGT C -3'	C28A/C32A/C35A
C28A/C32A/C35A/D319C reverse	5'- GAC ATC CCC CCC AAC ATT TCT CAC GAC GAT C -3'	
C310A forward	5'- GAT GAA GGA GCC AGC TCG CTC CTG TGA TCG -3'	wild-type
C310A reverse	5'- CGA TCA CAG GAG CGA GCT GGC TCC TTC ATC -3'	
C310A/C313A forward	5'- GCC AGC TCG CTC CGC TGA TCG TCG TGA G -3'	C310A
C310A/C313A reverse	5'- CTC ACG ACG ATC AGC GGA GCG AGC TGG C -3'	
C268A forward	5'- GGA AAG TCT TAC CTG CCC ACG CTG CTG AGA C -3'	wild-type
C268A reverse	5'- GTC TCA GCA GCG TGG GCA GGT AAG ACT TTC C -3'	
C248A/C268A forward	5'- CAA ATA TCC TAA GGC GTG GCC GGG CGG TTG G -3'	C268A
C248A/C268A reverse	5'- CCA ACC GCC CGG CCA CGC CTT AGG ATA TTT G -3'	
C310A/C313A/C323A forward	5'- GAT TGG GGG GGA GCT CGC TGT CAA G -3'	C310A/C313A
C310A/C313A/C323A reverse	5'- CTT GAC AGC GAG CTC CCC CCC AAT C -3'	
C310A/C313A/C323A /C325A forward	5'- GGG AGC TCG CGC TCA AGC ATT GGC CTT AAC -3'	C310A/C313A/C323A
C310A/C313A/C323A /C325A reverse	5'- GTT AAG GCC AAT GCT TGA GCG CGA GCT CCC -3'	

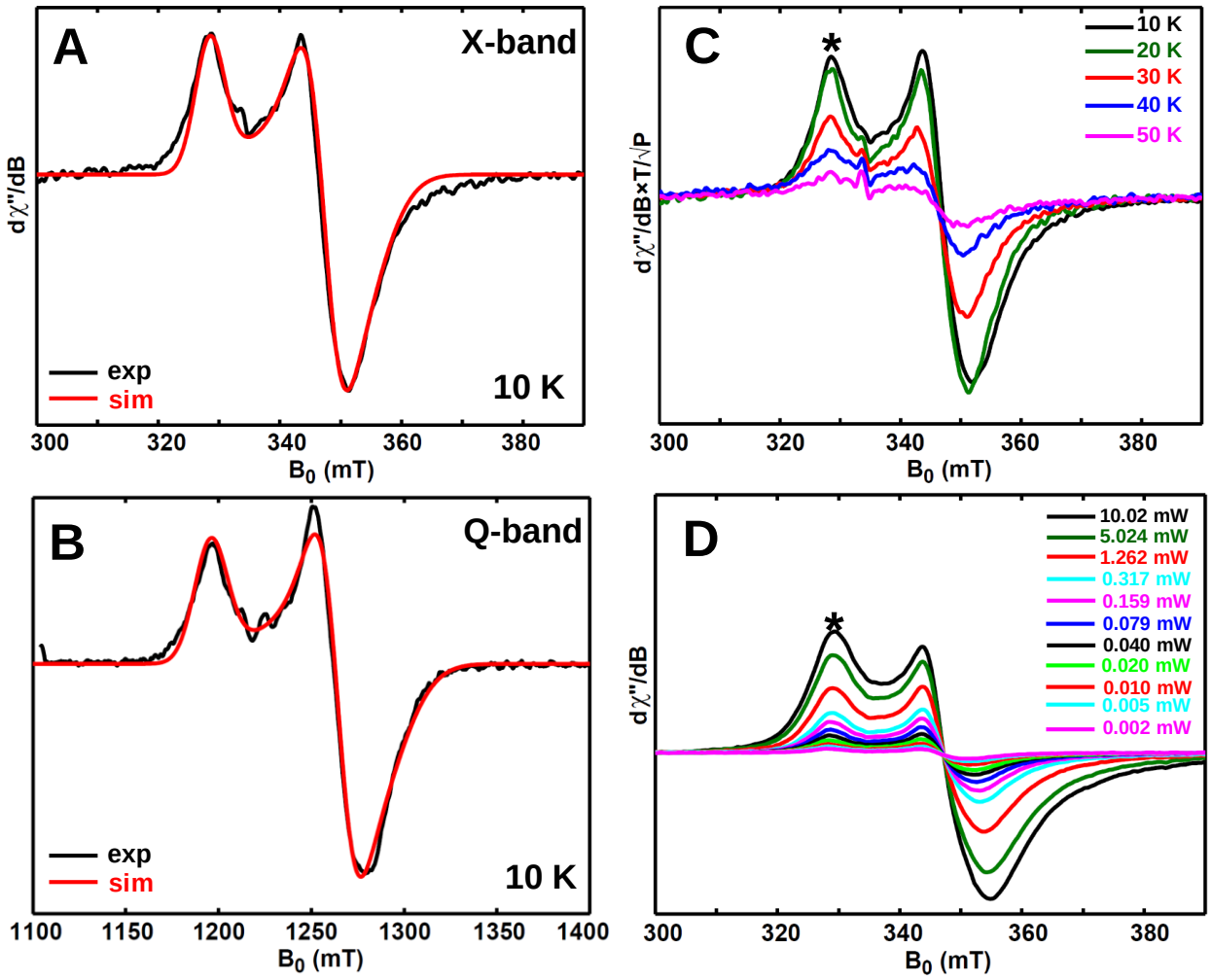

Figure S1. X-band (9.38 GHz) CW EPR (A) and Q-band (34.0 GHz) pseudo-modulated electron spin-echo detected field-swept EPR spectra (B) of dithionite-reduced double-knockout PqqE variant of *RS only*. The black traces are experimental spectra, while the red traces are the simulated spectra by employing the *g*-values = [2.040, 1.927, 1.897]. The X-band CW EPR spectra was recorded at 10 K, with 0.02 mW microwave power (no saturation). The Q-band EPR spectra was recorded at 10 K by using a two-pulse sequence of $\pi/2$-τ-π-τ-echo, with $\pi/2$ = 12 ns and τ = 300 ns. The modulation amplitude of 3.0 mT was used to convert the absorption spectra to the pseudo-modulated spectra in (B).
Temperature dependence (C) and power dependence (D) of the EPR signals of dithionite-reduced *RS-only* variant. The asterisk indicates the g_1 2.040 position, where the peak amplitudes are employed as the signal intensities of the RS cluster shown in Figure 4 (blue diamonds).

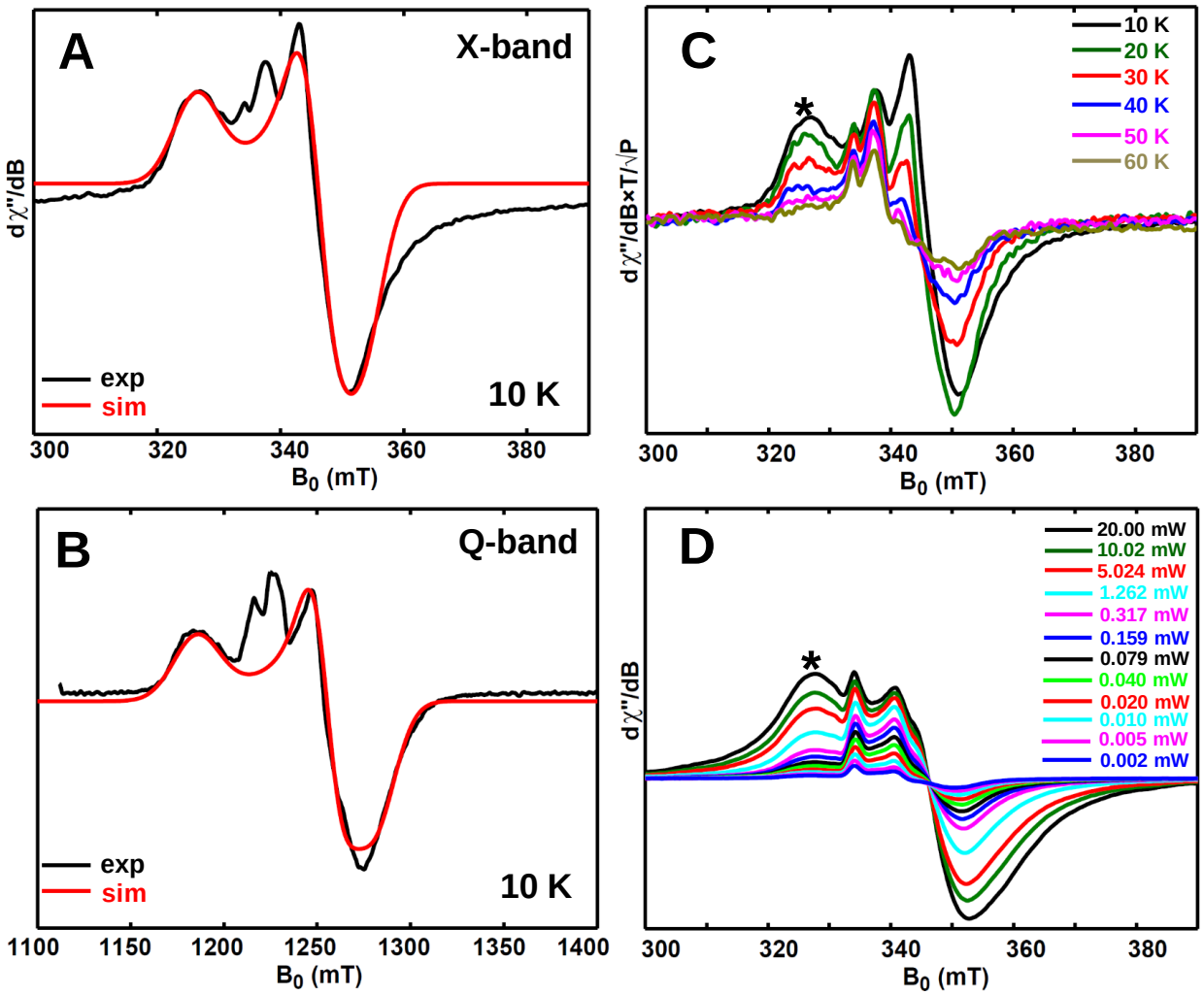

Figure S2. X-band (9.38 GHz) CW EPR (A) and Q-band (34.0 GHz) pseudo-modulated electron spin-echo detected field-swept EPR spectra (B) of dithionite-reduced *AuxI/AuxII*. The black traces are experimental spectra, while the red traces are the simulated spectra by employing the *g*-values = [2.059, 1.940, 1.903]. The X-band CW EPR spectrum was recorded at 10 K, with 0.02 mW microwave power (no saturation). The Q-band EPR spectrum was recorded at 10 K by using a two-pulse sequence of π/2-τ-π-τ-echo, with π/2 = 12 ns and τ = 300 ns. The modulation amplitude of 3.0 mT was used to convert the absorption spectra to the pseudo-modulated spectra in (B).

Temperature dependence (C) and power dependence (D) of the EPR signals of dithionite-reduced *AuxI/AuxII*. The asterisk indicates the g_1 2.059 position, where the peak amplitudes are employed as the major-component signal intensities of the AuxII cluster shown in Figure 4 (magenta squares).

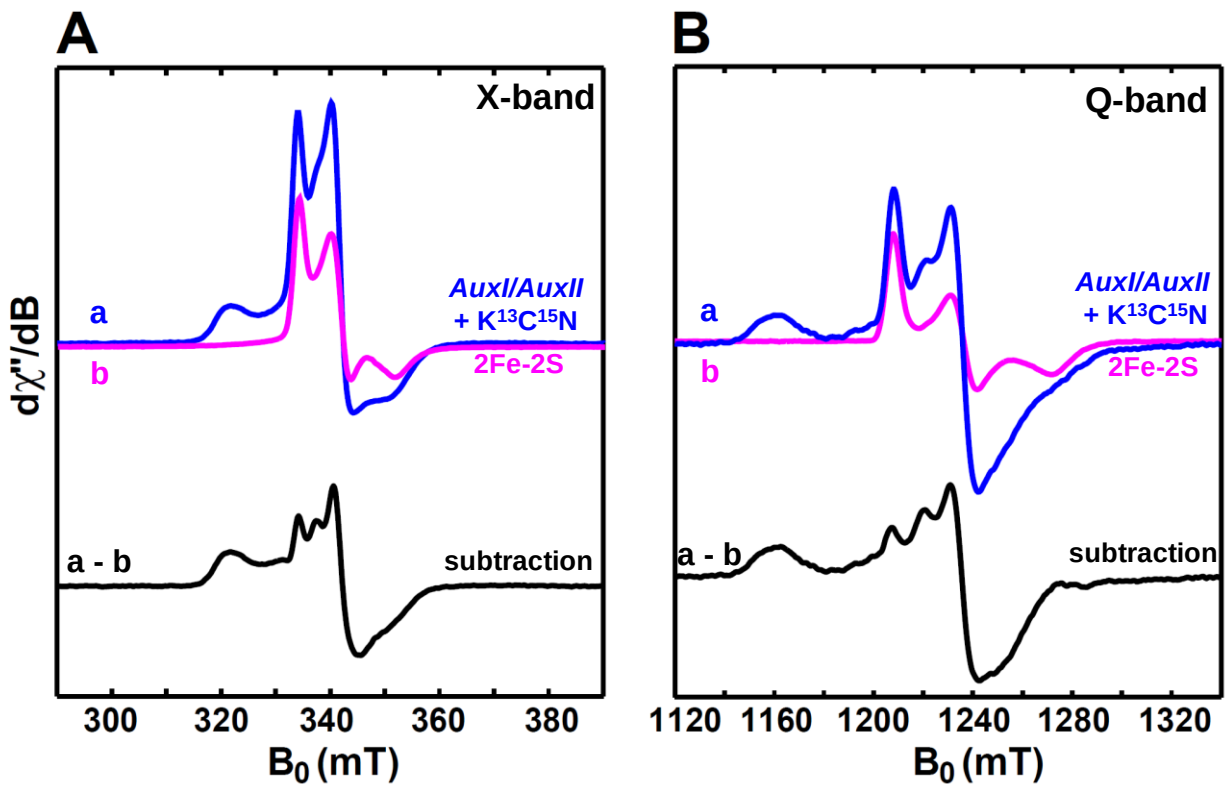

Figure S3. X-band (9.37 GHz) CW EPR (A) and Q-band (34.0 GHz) pseudo-modulated electron spin-echo detected field-swept EPR spectra (B) of dithionite-reduced *AuxI/AuxII* sample with the addition of ~100 equivalents of $K^{13}C^{15}N$. The blue traces are the original spectra, showing that the $[2Fe\text{-}2S]^{+}$ cluster signal was observed upon the $K^{13}C^{15}N$ addition. The black traces are the spectra we show in Figure 6, with the $[2Fe\text{-}2S]^{+}$ signal being subtracted away. The $[2Fe\text{-}2S]^{+}$ cluster signal (magenta traces) is adopted from the high-temperature EPR spectra of dithionite-reduced *RS/AuxI* (Figure S13), where only the $[2Fe\text{-}2S]^{+}$ cluster signal is persisting due to its slow-relaxation properties.

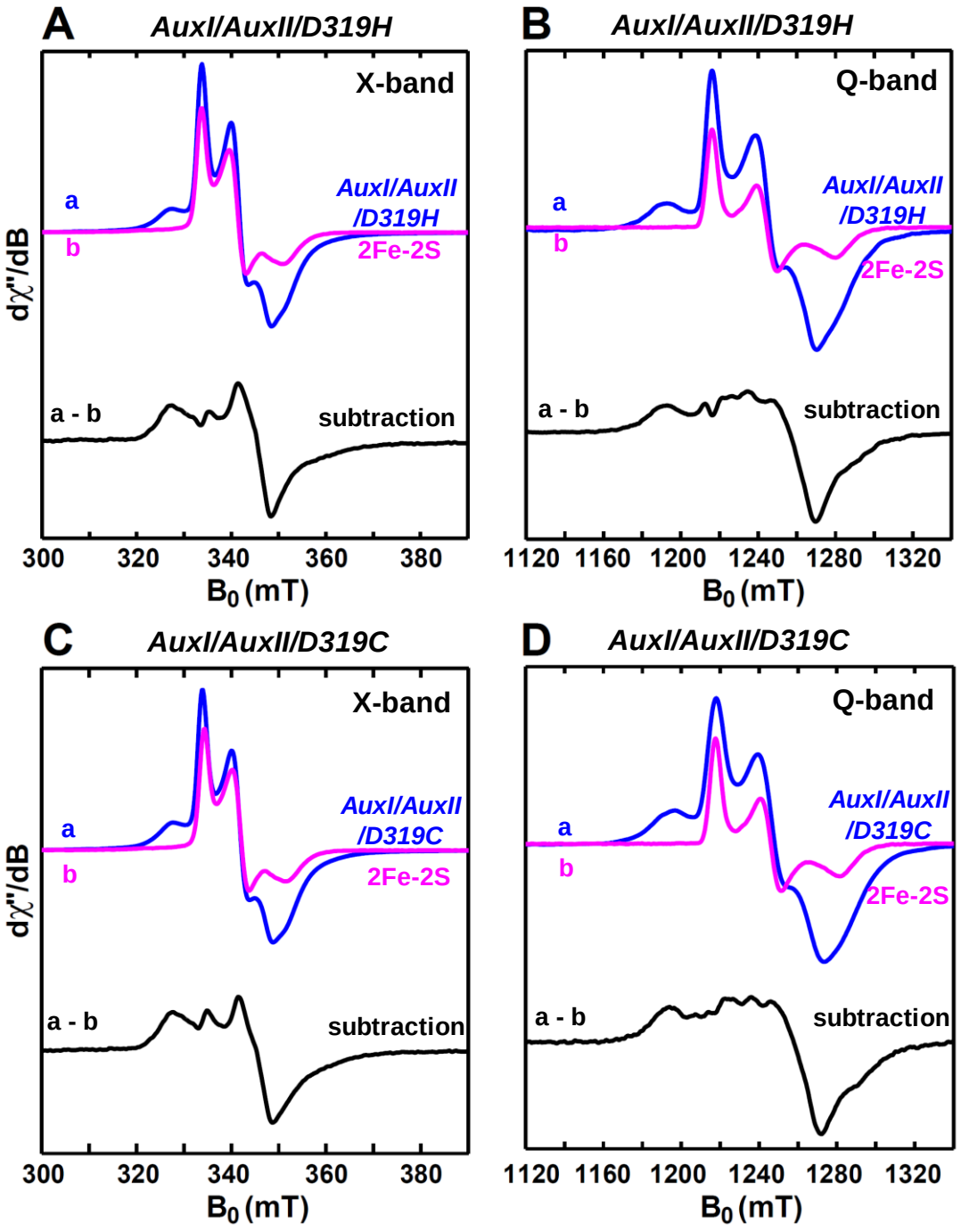

Figure S4. X-band (9.37 GHz) CW EPR (A, C) and Q-band (34.0 GHz) pseudo-modulated electron spin-echo detected field-swept EPR spectra (B, D) of dithionite-reduced *AuxI/AuxII/D319H* and *AuxI/AuxII/D319C*. The blue traces are the original spectra, showing that the $[2Fe\text{-}2S]^{+}$ cluster signal was observed. The black traces are the spectra we show in Figure 6, with the $[2Fe\text{-}2S]^{+}$ signal being subtracted away.

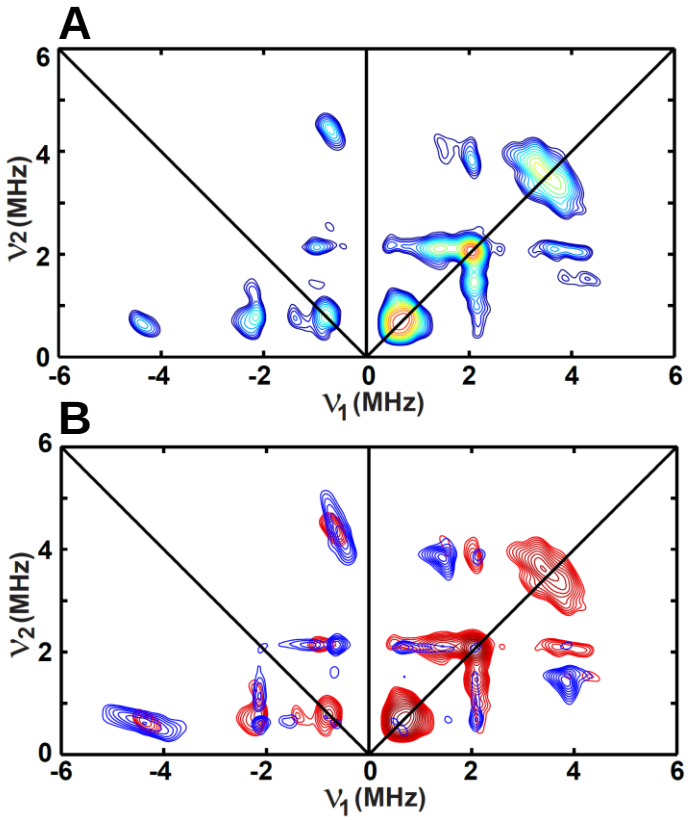

Figure S5. (A) X-band (9.403 GHz) HYSCORE spectra of dithionite-reduced *AuxI/AuxII/D319H* acquired at the magnetic field position (328.4 mT) corresponding to the *g*-value of 2.046. This spectrum is also shown in Figure 8C.
(B) The simulated ^{14}N-HYSOCRE spectrum are shown in blue (contour plot) by using the parameters of g = [2.087, 1.955, 1.941]; $A(^{14}N)$ = [0.73, 3.25, 1.01MHz, Euler angle = [55, 100, 25]° referring to **A** tensor to **g** tensor, $P(^{14}N)$ = [0.23, -1.02, 0.79] MHz, Euler angle = [50, 27, 20]° referring to **P** tensor to **A** tensor. The quadrupole coupling values we report here are defined as $[P_1, P_2, P_3] = e^2Qq/4I(2I\text{-}1)h[-1+\eta, 2, -1-\eta]$, with the asymmetry parameter η = 0.55.

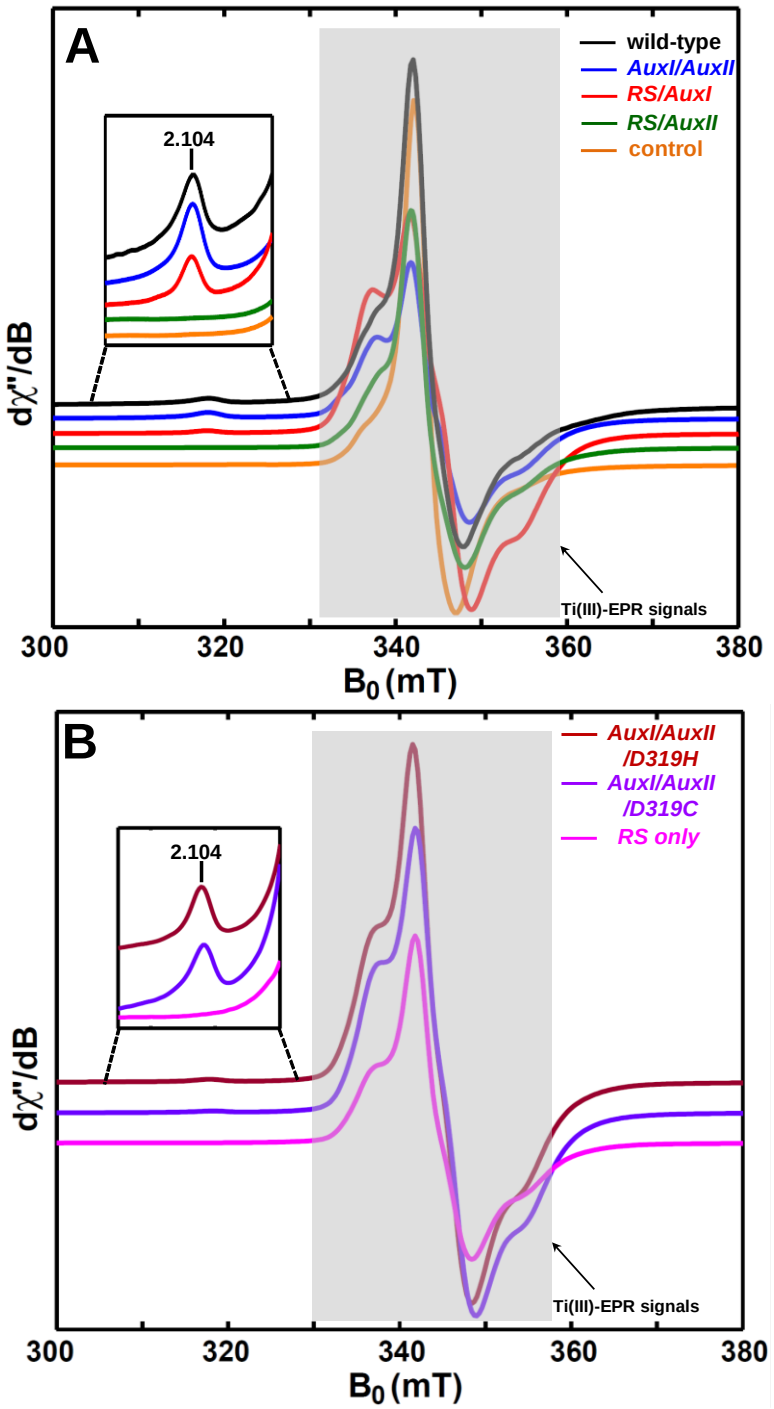

Figure S6. X-band (9.37 GHz) CW EPR spectra of Ti(III) citrate-reduced PqqE samples of wild-type (black trace), *AuxI/AuxII* (blue trace), *RS/AuxI* (red trace), *RS/AuxII* (green trace), *AuxI/AuxII/D319H* (burgundy trace), *AuxI/AuxII/D319C* (purple trace) and *RS only* (magenta trace). The control sample (orange trace) is Ti(III) citrate in HEPES-buffered solution. The CW EPR spectra were recorded at 10 K using 2.518 mW microwave power (no saturation).

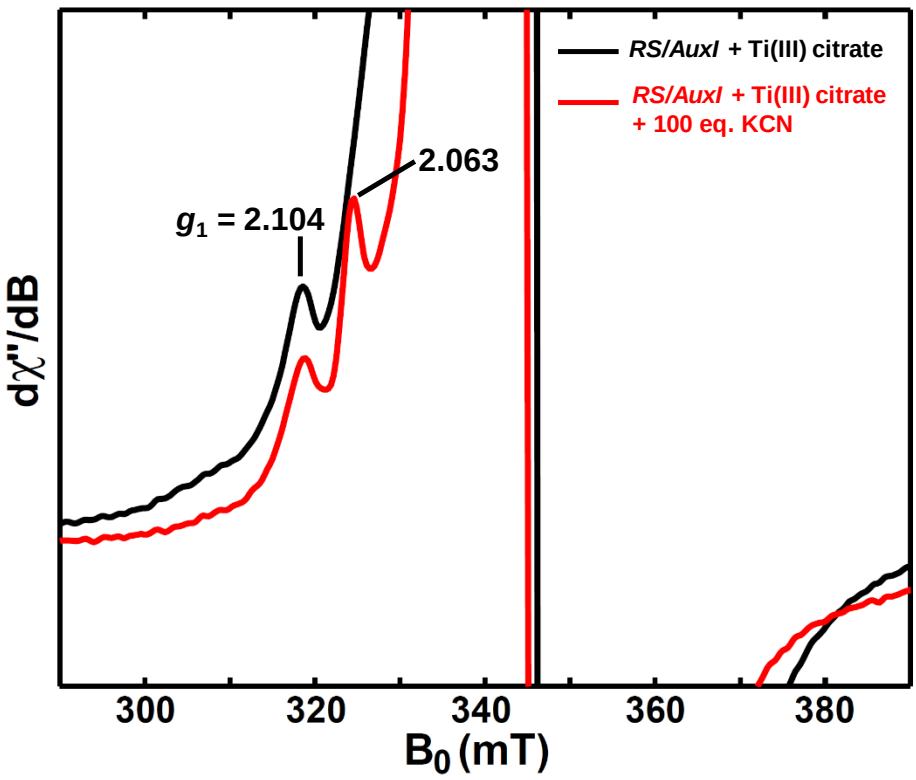

Figure S7. X-band (9.37 GHz) CW EPR spectra of Ti(III) citrate-reduced *RS/AuxI* PqqE variant (black trace) before (black trace) and after the addition of 110 equivalents of $K^{13}C^{15}N$. The CW EPR spectra were recorded at 10 K using 2.518 mW microwave power (no saturation). The signal with g = 2.063 arises from the CN-bound $[4Fe–4S]^{+}_{RS}$ species, as described in section of Characterization of the Radical SAM $[4Fe-4S]_{RS}$ Cluster.

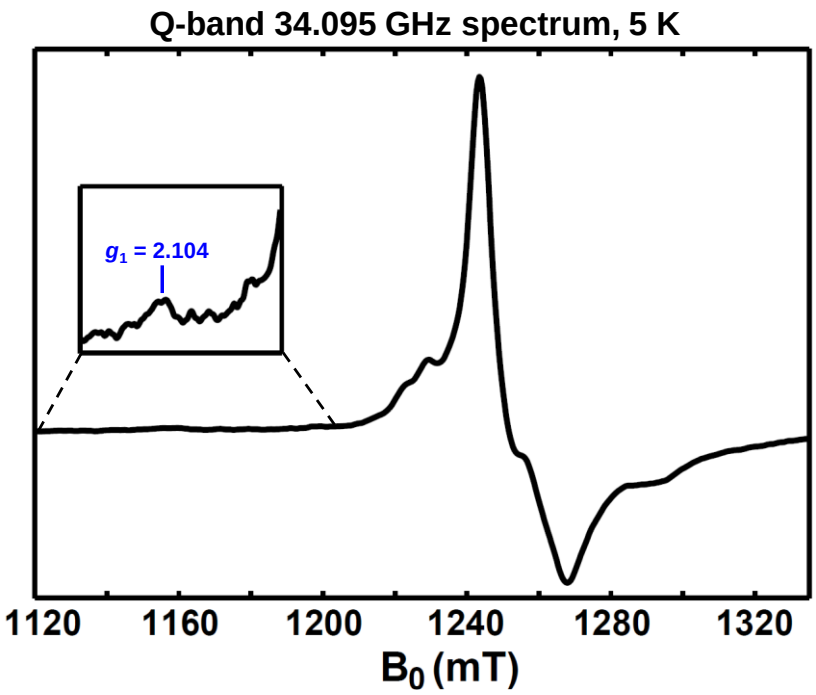

Figure S8. Q-band (34.0 GHz) pseudo-modulated electron spin-echo detected field-swept EPR spectrum of Ti(III) citrate-reduced wild-type PqqE. The spectrum was recorded at 5 K by using a two-pulse sequence of π/2-τ-π-τ-echo, with π/2 = 12 ns and τ = 300 ns. The modulation amplitude of 3.0 mT was used to convert the absorption spectrum to the pseudo-modulated spectrum.

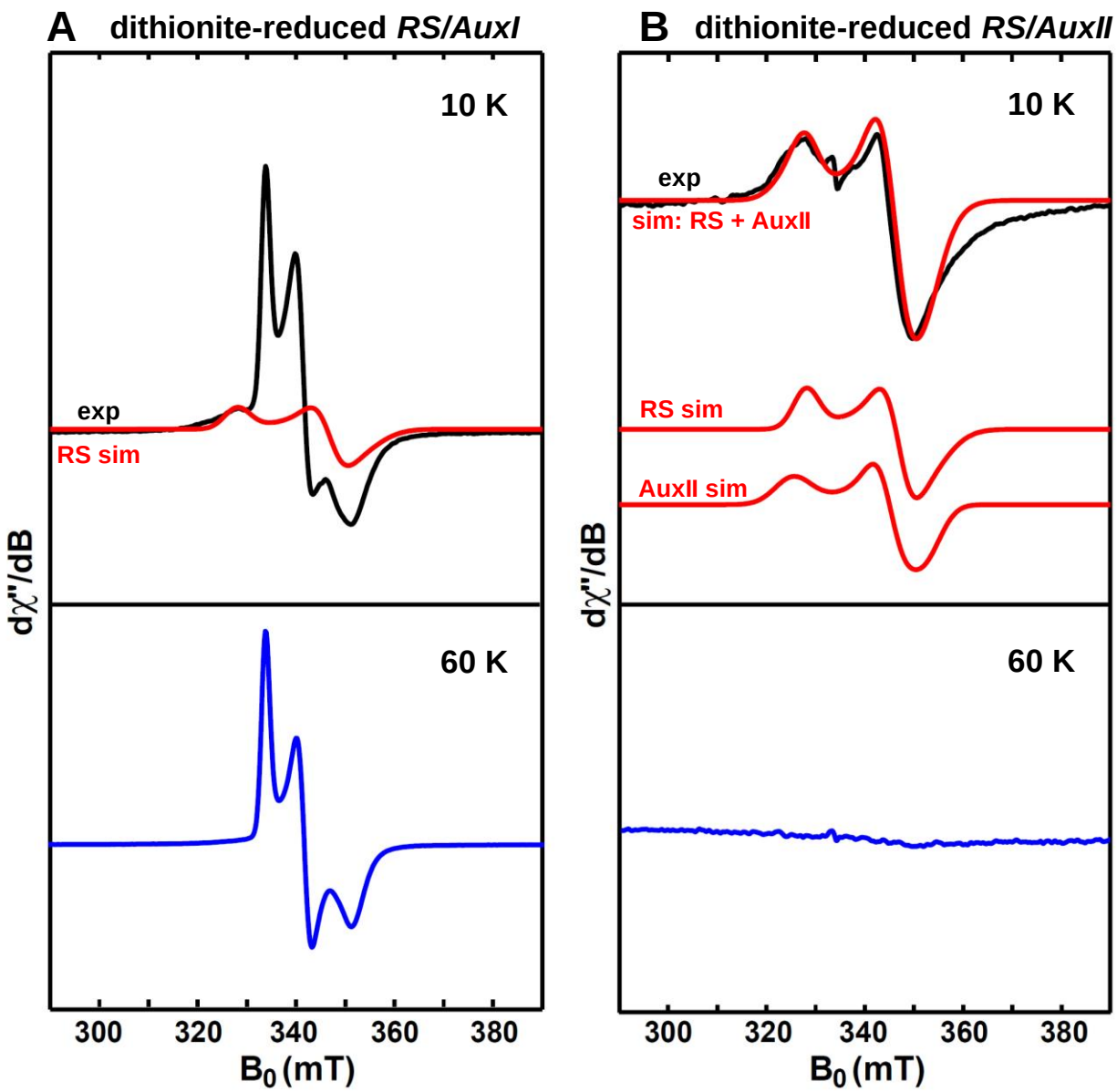

Figure S9. X-band (9.37 GHz) CW EPR spectra of dithionite-reduced *RS/AuxI* (A) and *RS/AuxII* (B). The experimental spectrum in (A, black trace) is dominated by the [2Fe-2S]$^{+}$ cluster signal, as well as the observable component that can be simulated by using the *g*-values = [2.040, 1.927, 1.897], corresponding to the RS cluster signal.
The experimental spectrum in (B, black trace) has two components. This spectrum can be well simulated by employing two components with the ratio of 1:1; one corresponds to the RS cluster with *g*-values = [2.040, 1.927, 1.897] and the other one is the AuxII cluster with *g*-values = [2.059, 1.940, 1.903].

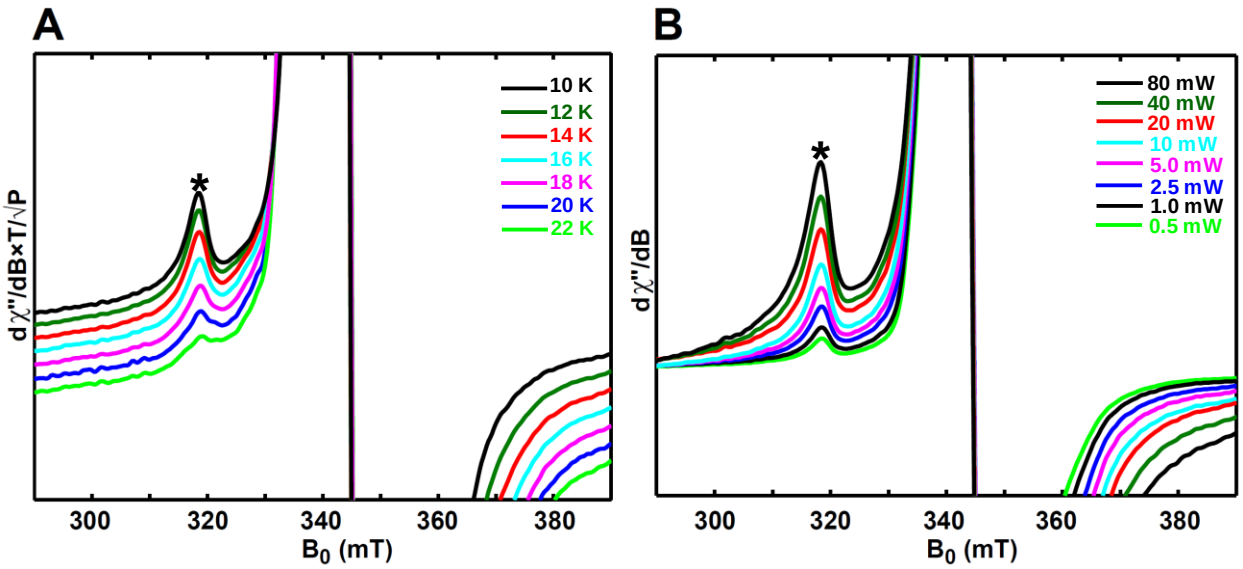

Figure S10. Temperature dependence (A) and power dependence (B) of the EPR signals of Ti(III) citrate-reduced WT PqqE. The asterisk indicates the g_1 2.104 position, where the peak amplitudes are employed as the signal intensities of the AuxI $[4Fe\text{-}4S]^{+}$ cluster shown in Figure 4 (red circles).

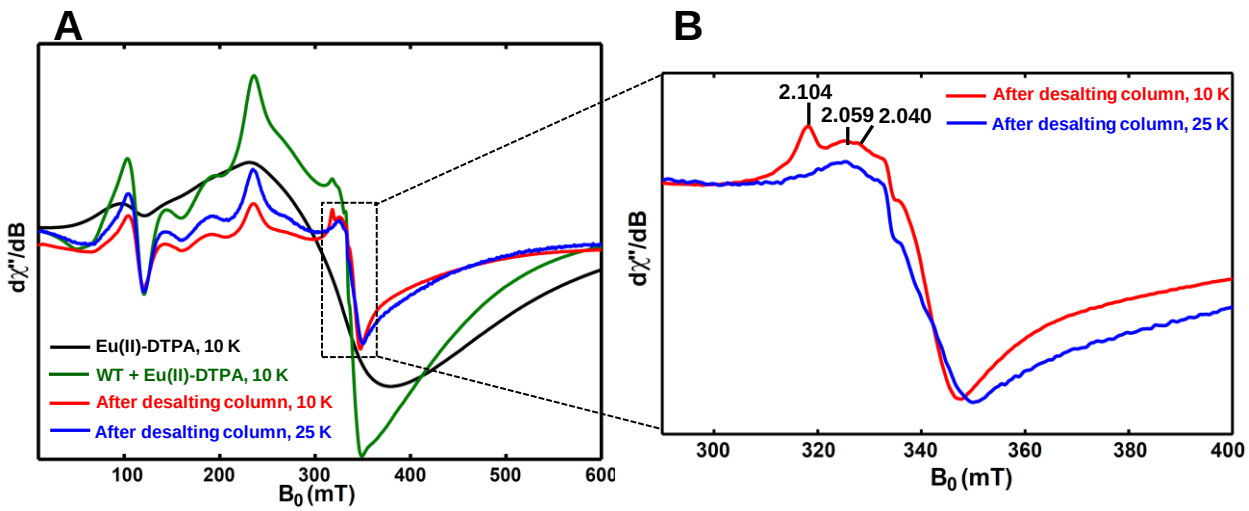

Figure S11. X-band (9.37 GHz) CW EPR spectra of Eu(II)-DTPA-reduced wild-type PqqE before and after desalting. The g_1 value of 2.104, 2.059 and 2.040 is corresponding to the AuxI $[4Fe–4S]^+$ cluster, the AuxII $[4Fe–4S]^+$ cluster and the RS $[4Fe–4S]^+$ cluster, respectively. The g_1 2.004 of $[2Fe–2S]^+$ is not well resolved due to the overlap in the central region. The CW EPR spectra were recorded by using 2.518 mW microwave power at 10 K.

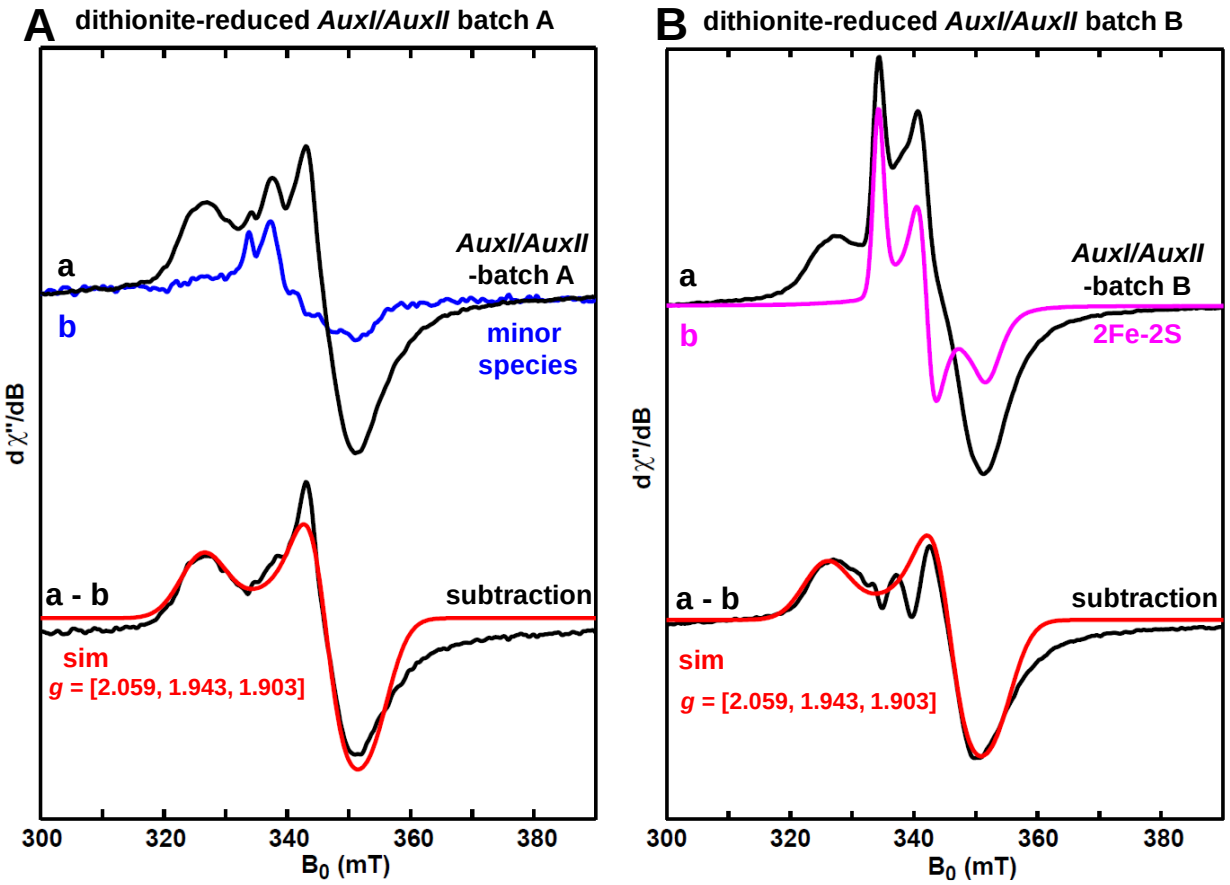

Figure S12. X-band (9.37 GHz) CW EPR of dithionite-reduced two batches of the *AuxI/AuxII* samples. The batch A spectrum is shown in Figure 6.

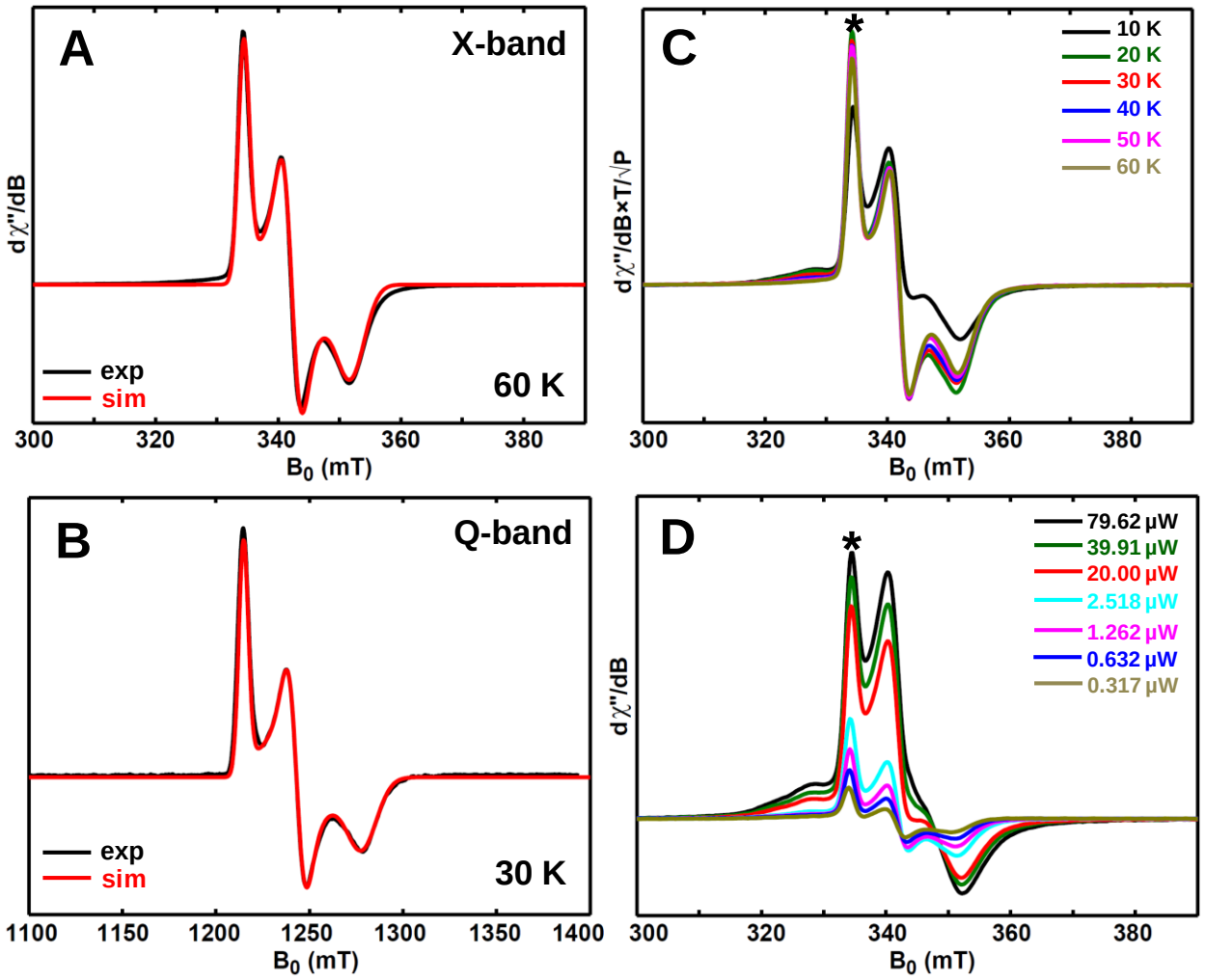

Figure S13. High temperature X-band (9.38 GHz, 60 K) CW EPR (A) and Q-band (34.0 GHz, 30 K) pseudo-modulated electron spin-echo detected field-swept EPR spectra (B) of dithionite-reduced *RS/AuxI*, showing only the $[2Fe\text{-}2S]^{+}$ cluster signals. The black traces are experimental spectra, while the red traces are the simulated spectra by employing the *g*-values = [2.004, 1.958, 1.904]. The CW EPR spectra were recorded at 60 K, with 0.02 mW microwave power (no saturation). The Q-band EPR spectra were recorded at 30 K by using a two-pulse sequence of $\pi/2$-τ-π-τ-echo, with $\pi/2$ = 12 ns and τ = 300 ns. The modulation amplitude of 3.0 mT was used to convert the absorption spectra to the pseudo-modulated spectra in (B).
Temperature dependence (C) and power dependence (D) of the EPR signals of dithionite-reduced *RS/AuxI* at 10 K. The asterisk indicates the g_1 2.004 position, where the peak amplitudes are employed as the signal intensities of the $[2Fe–2S]^{+}$ cluster (green triangles) shown in Figure 4. The small amount signal intensity from the RS cluster is omitted.